Byproduct-Based Ettringite Binder – A Synergy Between Ladle Slag and Gypsum

Hoang Nguyen [a*], Elijah Adesanya [a], Katja Ohenoja [a], Lubica Kriskova [b], Yiannis Pontikes [b], Paivo Kinnunen [a], Mirja Illikainen [a]

[a] *Fibre and Particle Engineering Research Unit, University of Oulu, Pentti Kaiteran katu 1, 90014 Oulu, Finland*

[b] *KU Leuven, Department of Materials Engineering, Kasteelpark Arenberg 44, 3001 Leuven, Belgium*

* Corresponding author email: hoang.nguyen@oulu.fi

Abstract

Ladle slag (LS) is a byproduct from the steel industry that is usually reactive on its own and hydrates towards cementitious phases when mixed with water. However, these reaction products are often metastable, leading to micro-structural changes between 7 and 30 days after mixing. To address this issue, in this experimental investigation, a new binder was designed where LS was mixed with gypsum in order to deliver an ettringite-based binder (LSG). The experimental results revealed that the dominant crystalline phase of LSG was ettringite, which

remained stable with no conversion at later stages. For better understanding of the ettringite-based binder, mortar characterization, mechanical properties, and durability of LSG were investigated. LSG showed good mechanical properties and excellent freeze-thaw resistance after 300 cycles, which is comparable to other calcium sulfoaluminate cements. Therefore, as a result, the byproduct-based ettringite binder synthesized herein could offer a solution to steelmaking byproducts with a low-CO_2 binder, which could be used in a wide range of applications in the construction industry.

***Keywords**:*

Recycling; Eco-cement; Calcium sulfoaluminate; Sustainability; CO_2 emission; Ladle slag

1. Introduction

Ladle slag (LS) is an industrial byproduct from steel manufacturing processes, which currently is mostly disposed to landfills or used in low-value applications [1,2]. According to a statistical report from the World Steel Association [3], 2.1–2.6 million tons of LS is produced in Europe annually, if every ton of crude steel results in 12–15 kg of unrecycled LS. LS can be used as a supplementary cementitious material or cement clinker production [4]; however, a high replacement ratio is not recommended because LS may reduce the strength of concrete [5]. Furthermore, LS often suffers from self-pulverization, which leads to several potential challenges (e.g., handling and storing difficulties) [6]. In our previous research, LS has shown promising properties as an Al-rich precursor for alkali-activated materials (AAM) [7,8]. The

alkali-activated LS attained up to 70 MPa compressive strength [7] with appropriate durability [8]. Additionally, LS has been successfully used as co-binder to produce a foam cement for energy-saving buildings [9], or as high-temperature AAM [10].

AAM is often an eco-friendly material with up to 80% lower CO_2 footprint compared to the ordinary Portland cement (OPC) [11,12]. However, depending on feedstock sources and transportation costs, the cost and greenhouse gas emission of AAM can be comparable to that of typical OPC concretes [13,14]. The main sources of the CO_2 emissions (and cost) in AAM are related to the production of the alkali activators (mainly sodium hydroxide and sodium silicate), including mining, treatment, and transportation of raw materials using in the manufacturing processes [15]. Suggestions have been put forward in the literature, e.g. alternative activators will contribute to decreased environmental impacts for AAM [16]. For that reason, slag cements with minimized alkali-activator content are of high interest.

An interesting alternative is to use LS as a precursor for ettringite-based binders in which ettringite ($C_3A \cdot 3C\bar{S} \cdot 32H$) is the main reaction product. Ettringite is formed by the reaction between solid calcium aluminate and calcium sulfate. Calcium sulfoaluminate belite cement (CSAB) and supersulfated cement (SSC), both which can be produced from byproducts, such as fly ash and blast furnace slag [17,18], are the most popular ettringite-based binders. These residue-based binders have lower CO_2 emissions while offering comparative mechanical performance in comparison to OPC [17,18]. LS has been successfully used as a precursor to

produce an ettringite system through reactions with dehydrated gypsum ($CaSO_4$) [19]. Although the material showed promising properties (e.g., appropriate setting time, good compressive strength), the preparation process was sub-optimal as it necessitated uneconomical steps, such as re-melting and rapid cooling of the slag. Furthermore, dehydrated gypsum ($CaSO_4$) was used instead of hydrated gypsum ($CaSO_4 \cdot 2H_2O$), which is available as a secondary resource. The use of hydrated gypsum reduces energy consumption in the dehydration process in comparison to dehydrated gypsum.

Encouraged by a need for a new eco-friendly binder and better utilization for LS, this experimental investigation aimed to develop a novel ettringite-based binder from the hydration between LS and hydrated gypsum ($CaSO_4 \cdot 2H_2O$). The binder produced here resulted from a reaction between naturally-cooled LS and hydrated gypsum. The only processing step needed was grinding of LS to similar particle size as OPC. Hence, the energy demand to produce the material was relatively low. To assess the quality of the hydrated ladle slag cements, the mechanical properties and durability of hydrated LS with and without gypsum (abbreviated as LSG and HLS, respectively) were investigated.

2. Materials and Methods

2.1. Materials

The LS was supplied by SSAB Europe Oy (Raahe, Finland). The slag was collected at the

77 slag cooling pit of the company, where the material has been exposed to natural weather
78 conditions. The chemical composition of the LS, as shown in Table 1, was analyzed by X-ray
79 fluorescence (XRF) (PANalytical Omnian Axiosmax) at 4 kV. The free CaO measured by the
80 method described in the standard EN 450-1 [20] was zero. After characterization, the as-
81 received LS was milled with a ball mill (TPR-D-950-V-FU-EH by Germatec, Germany) to
82 reach a d_{50} value of less than 10 μm as recommend in [7]. The particle size distribution was
83 measured by a laser diffraction technique (Beckman Coulter LS 13 320) using the Fraunhofer
84 model [21]. Quantitative XRD (QXRD) was undertaken to determine the amorphous and
85 crystalline content in the slag, analytical grade crystalline titanium oxide (10 wt.%) was added
86 to the slag as internal standard. The mineralogical content of the slag is reported in Table 1 and
87 Figure 1. It is worth noting that the polymorph of C_3A is cubic; as in XRD spectra (Figure 1),
88 there is a peak at a diffraction angle of around 33.5° [22].

89 ***Table 1. Mineralogy content (wt %) of LS measured by QXRD***

Oxide	γ-C_2S	C_3A	$C_{12}A_7$	MgO	Amorphous
LS	22.6	11.5	26.9	13.0	15.9

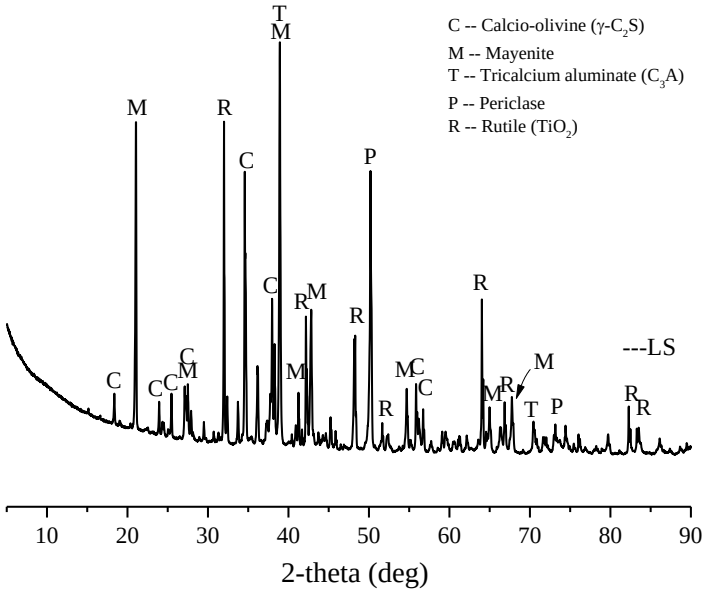

Figure 1. XRD characterization of the as-received LS

A commercially available gypsum ($CaSO_4 \cdot 2H_2O$) supplied by VWR Finland (product code 22451.360) was used as a calcium sulfate source in this study. The particle size distribution of gypsum was measured by the same equipment and technique with LS; the median particle size d_{50} was 11.5 μm. Furthermore, XRF was used to assess its chemical composition (see Table 2). It is expected that gypsum will react with mayenite ($C_{12}A_7$) in the unhydrated LS to form ettringite ($C_3A \cdot 3C\bar{S} \cdot 32H$) [19]. The reaction between $C_{12}A_7$ and gypsum is as follow:

$$C_{12}A_7 + 12C\bar{S} \cdot 2H + 137H \rightarrow 4C_3A \cdot 3C\bar{S} \cdot 32H + 3AH_3 \quad (1)$$

Table 2. Chemical composition (wt %) of LS measured by XRF

Oxide	CaO	SiO_2	Al_2O_3	Fe_2O_3	MgO	SO_3	Others
Nomenclature	*C*	*S*	*A*	*F*	-	$\bar{S}$	-
LS	51.0	8.3	27.9	1.1	6.3	0.8	4.6

Gypsum	41.4	1.0	0.1	0.1	0.5	53.8	3.1

Due to the fast setting properties of $C_{12}A_7$ in the LS, citric acid (product code C1949 by Tokyo Chemical Industry Co., Ltd., Japan) was used as a retarder to prolong the workability of the matrix. Based on preliminary results, 0.8 wt% (to water) citric acid solution was used to attain almost 1 hour before initial setting time. The anhydrous citric acid was mixed with water at roughly 300 rpm for about 20 minutes. Automatic Vicat machine (model E044N by Matest, Italy) was employed to record the setting time of the mortars complying with ASTM C191 [23]. A standard sand (DIN EN 196-1) was used in this study to prepare mortar samples.

2.2. Methods

2.2.1. Sample preparation and analysis

The required amount of gypsum to fully complete the reaction of $C_{12}A_7$ was calculated to be 30 wt% using the modified Bogue equation as proposed in [19]. LS and gypsum were initially blended for 3 minutes, after which citric acid-water solution and sand were added in a 5-liter mixer at low (roughly 70 rpm) and high (roughly 150 rpm) speed following EN-196 [24]. Mortar samples were cast into 40 × 40 × 160 mm^3 molds and vibrated for two minutes at a frequency of 1 Hz. Samples were cured in plastic bags at room temperature for 24 hours before demolding. Samples were then cured in a water bath at room temperature (approximately 23°C) until testing (7 and 28 days). The mixture composition/proportion is shown in Table 3. For HLS samples, the procedure was the same with LSG but without adding

gypsum.

Table 3. Mix proportions (in gram) of the LSG and HLS

ID	Slag	Gypsum	Sand	Water*
HLS	450	-	1350	202.5
LSG	315	135	1350	202.5

*water-to-binder ratio was 0.45

Quantitative X-ray diffraction (QXRD) data was collected for LSG paste samples using Rigaku SmartLab 9 kW. The analysis employed Co Kα radiation (Kα1 = 1.78892 Å; Kα2 = 1.79278 Å; Kα1/Kα2 = 0.5), at a scan rate of 3°/min in the range 5°-90° (2θ), and 0.02°/step. Phase identification was done using "X'pert HighScore Plus" (PANalytical software) and for the Reitveld quantitative phase analysis. Due to unidentifiable coordination, QXRD/Rietveld analysis for HLS paste sample was not possible to quantify the changes in mineralogy at both 7 and 28 days. SEM observation was done for paste samples on Zeiss Sigma using a secondary electron detector with a voltage of 5–15 kV. Precisa Gravimetrics AG "prepASH automatic drying and ashing system" was used for thermogravimetric analysis (TGA-DTG). Crushed samples of similar mass were transferred to crucibles and heated from 23 to 1000 °C at 10 °C/min in a nitrogen atmosphere to detect the change in mass. Isothermal calorimetry analysis was undertaken at room temperature (23 °C) for the two mixtures to study the heat evolution at early hydration times. A TAM Air instrument was used, the samples were mixed

133 in-situ and the measurement lasted up to 50 hours.

134 **2.2.2. Mechanical and durability tests**

135 The mechanical properties of HLS and LSG measured included flexural and compressive
136 strength; the volume stability was also analyzed for the hardened mortar with drying shrinkage.
137 The three-point bending and compressive strength tests, according to the standard [24], were
138 conducted after 7 and 28 days of curing, employing a Zwick mechanical testing instrument
139 with a load cell of 100 kN. The three-point bending test was done using force control at 0.05
140 kN/s for two parallel samples. The compressive strength was measured by loading the halves
141 of the prismatic bending specimens. At least four specimens were tested, and the force speed
142 was set at 2.4 kN/s.

143 Drying shrinkage measurements were carried out on duplicate prism samples with
144 dimensions of 40 × 40 × 160 mm^3 cured at room temperature and relative humidity of 60%,
145 according to ASTM C596 [25]. The length measurement was carried out using a Matest E077
146 kit length comparator at the age of 1, 3, 7, 14, 28 and 90 days after casting. The length change
147 (*LC*) over time was then calculated using Equation 2.

$$LC(\%) = \frac{\mathrm{L}_i - L_x}{G} \times 100 \quad (2)$$

148 Where L_i is the difference between the comparator reading and the reference bar at 3 days, L_x
149 is the length at each curing age of the specimen and *G* is the nominal effective length.

150 The freeze-thaw resistance of HLS and LSG were assessed for better understanding about

151 the durability of materials. This investigation used a freezing and thawing testing scheme
152 modified according to ASTM C666 [26]. The specimens were kept half-immersed in water and
153 half in air for up to 300 cycles. Each cycle consists of reducing the temperature of the specimens
154 from 15 °C to -20 °C for 2 hours and maintaining at this temperature for 1 hour, and then raising
155 it from -20 °C to 15 °C for 2 hours and maintaining this temperature for 1 hour. The residual
156 compressive strength, weight loss and relative modulus of elasticity of HLS and LSG mortars
157 was determined after each 60 freeze-thaw cycles. Matest ultrasonic pulse (Matest, Italy) was
158 used to determine pulse velocity (UPV) before freeze thaw and after each 60 cycles of freeze-
159 thaw. It is worth noting that UPV has shown an acceptable correlation with the compressive
160 strength of inorganic binders as reported in the literature [27,28]. The relative dynamic modulus
161 of elasticity (E_d) was then calculated using Equation 3 [29,30].

$$E_d = \frac{V_d^2}{V_0^2} \times 100 \quad (3)$$

162 where V_n is the ultrasonic pulse velocity after n cycles and V_0 at 0 cycles.

163 **3. Results and Discussion**

164 **3.1. Phase structure and composition**

165 LSG formed mainly ettringite as its crystalline hydration product (see Figure 2) similar to
166 CSAB and SSC [17,18]. The QXRD pattern of LSG in Figure 2a clearly shows that ettringite
167 (AFt) is the dominant crystalline phase in the structure. In addition, LSG produced ettringite

quickly after the reaction among LS, gypsum, and water. Through Rietveld analysis, the calculated amount of ettringite produced at 7 days was determined to be roughly 34.4 wt.% of the total mineralogy of the paste. While this value slightly decreased at 28 days with an ettringite value recorded to be around 27.3 wt.% (Figure 2b). This may be probably due to the transformation of ettringite to calcium monosulfoaluminate (AFm) as further hydration occurs in the gypsum-slag mix. It is expected that the hydration of the anhydrous gypsum-slag cement would continue by reacting further with already formed ettringite to form AFm at extended hydration times [31]. This is consistent with the increased amount of AFm from 0.5 wt.% at 7 days to 5.3 wt.% at 28 days in Figure 2b. Consequently, the amorphous content of LSG increases gradually from 45.6 wt.% at 7 days to 46.7 wt.% after 28 days of hydration. This analysis shows that ettringite and an amorphous hydration product are the dominant hydrated product and thus the strength-giving phase in the material. From Equation 1, one of the anticipated hydration product of the reaction between mayenite and gypsum is gibbsite (AH_3). However, its detection in XRD is difficult to detect and possibly contributes to the amorphous content in the LSG sample. As in [32], AH_3 could offer higher indentation modulus, hardness, and compression strength to the ettringite-based binder.

On the other hand, HLS converted its hydrated products during the curing period. Diffractograms (Figure 2c) for HLS at 7 days shows dicalcium aluminate hydrate (C_2AH_8), and katoite (C_3AH_6) as the main hydration products. In high-calcium aluminate materials, the initial

187 hydration products are proposed to be metastable hydrates such as dicalcium aluminate hydrate
188 (C_2AH_8) and also AH_3 [33,34]. Due to it instability, C_2AH_8 crystals inevitably convert to stable
189 hydrates (i.e., C_3AH_6), with a change in volume. This phenomenon led to the strength loss of
190 the concrete at 28 days (as will be discussed in Section 3.3.1). Furthermore, the diffractograms
191 at 28 days show a notable reduction in the C_2AH_8 and an increase in the intensity of katoite,
192 which may suggest the conversion taken place. Furthermore, when this conversion occurs,
193 there is a release of water, which is available for supplementary hydration of $C_{12}A_7$ or the
194 anhydrous material in the slag [35]. Similar diffractograms of formation and reduction in peak
195 intensity can be found in studies on high-alumina cements by Chavda et al. [36] and Adesanya
196 et al. [37]. In addition, strätlingite existed in the diffractograms at 28 days; this may have
197 surfaced due to the increased alkalinity of the matrix during aging/reactions, which
198 subsequently leads to the hydration of silicon in the anhydrous or unreacted slag. In addition,
199 by using gypsum, the system formed ettringite through the reaction with $C_{12}A_7$ (see Equation
200 1), and hence eliminated the mineral conversion and related strength loss. Further identification
201 of these hydration products and conversion process are discussed providing more details in the
202 TGA-DTG analysis.

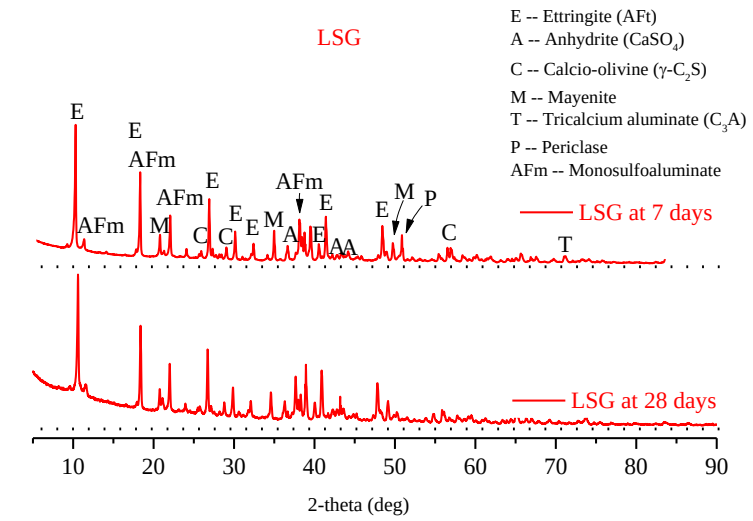
LSG
E -- Ettringite (AFt)
A -- Anhydrite (CaSO4)
C -- Calcio-olivine (γ-C2S)
M -- Mayenite
T -- Tricalcium aluminate (C3A)
P -- Periclase
AFm -- Monosulfoaluminate
LSG at 7 days
LSG at 28 days
2-theta (deg)

(a)

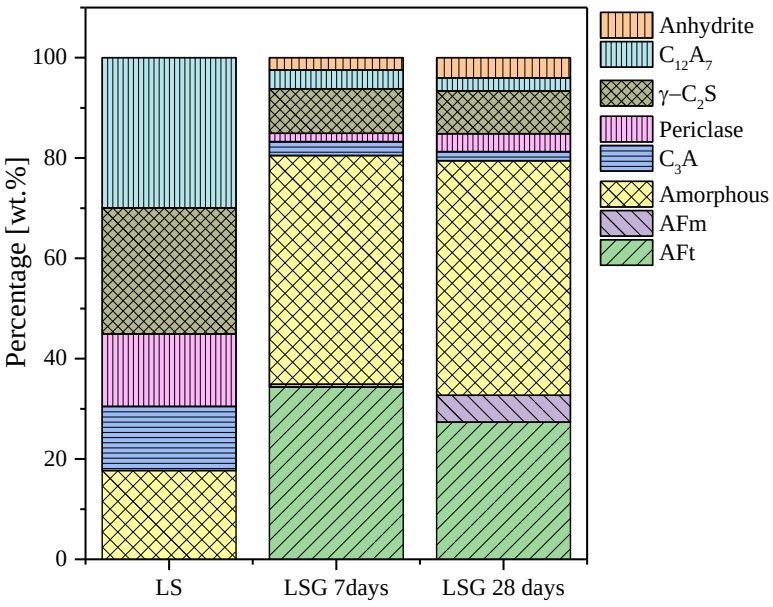
Anhydrite
C12A7
γ–C2S
Periclase
C3A
Amorphous
AFm
AFt
Percentage [wt.%]
LS
LSG 7days
LSG 28 days

(b)

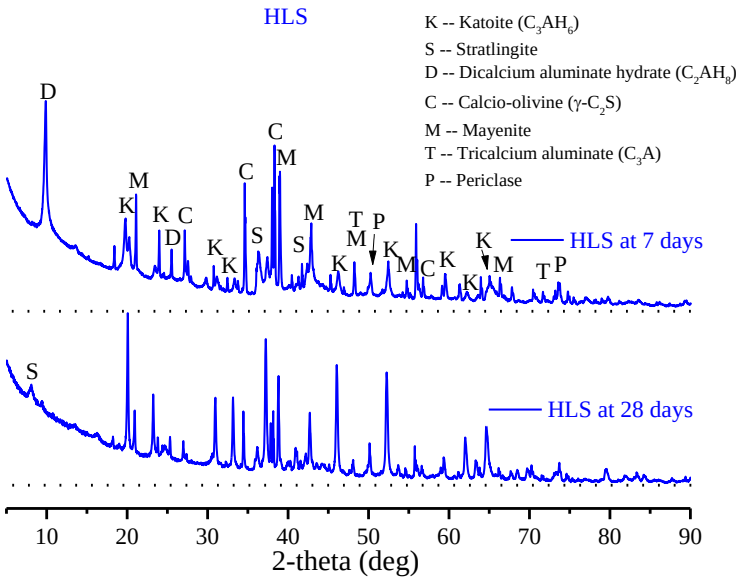

(c)

203 ***Figure 2. X-ray diffraction analysis for (a) LSG (b) QXRD of LSG and (c) HLS at 7 and 28***

204 ***days of curing.***

205 The thermogravimetric analysis in Figure 3 helps to identify the reacted phases and the

206 hydration products of the pastes. The analysis is consistent with the conversion mechanism of

207 the hydration products in HLS. For LSG at all ages, a well-defined endothermic peak can be

208 observed starting from 50 °C with a definite peak at 200 °C; this corresponds to the

209 decomposition of ettringite [38,39], which according to its chemical composition consists of

210 approximately 45% of water. A slight shoulder can be observed between 250-300 °C which

211 corresponds to the decomposition of poorly crystalline AH_3 [40]. It is noteworthy to know that

212 this shoulder between 250-300 °C is also identified with the formation of AFm and probably

213 overlaps [41]. As for HLS, two distinct endothermic peaks were noticeable at 180 and 350 °C

214 for both 7 and 28 days. The peak at 180 °C is attributed to the decomposition of the metastable

hydration product C_2AH_8, while the peak centered at 350 °C is attributed to the stable C_3AH_6 [40,42]. At early age, the intensity of C_2AH_8 peak is more profound than C_3AH_6. However, at 28 days, the intensity of the endotherm peak of C_3AH_6 increased, while that of C_2AH_8 reduced due to the conversion of the hydrates. This behavior is fully consistent with the proposed conversion process and is in agreement with the strength reduction at 28 days, detailed in Section 3.3.1.

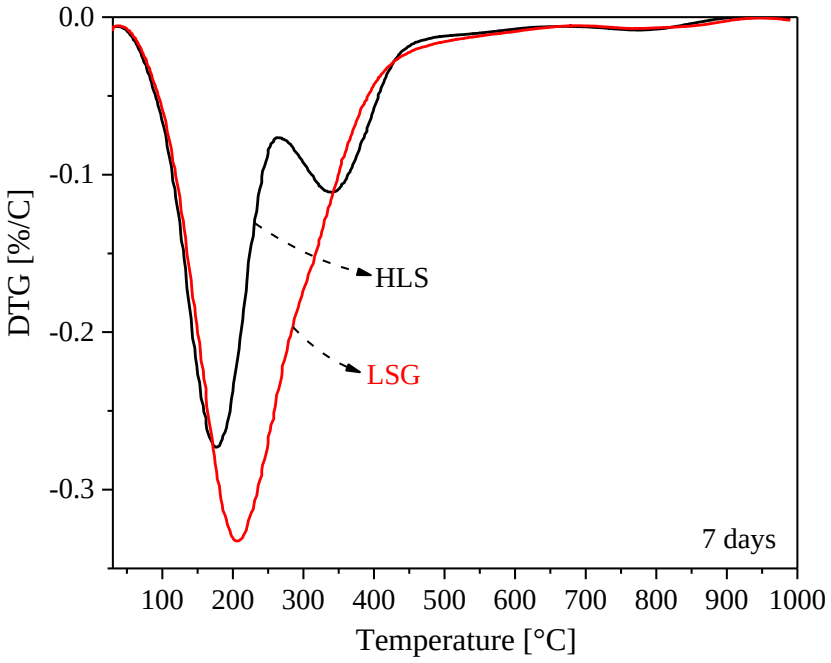

(a)

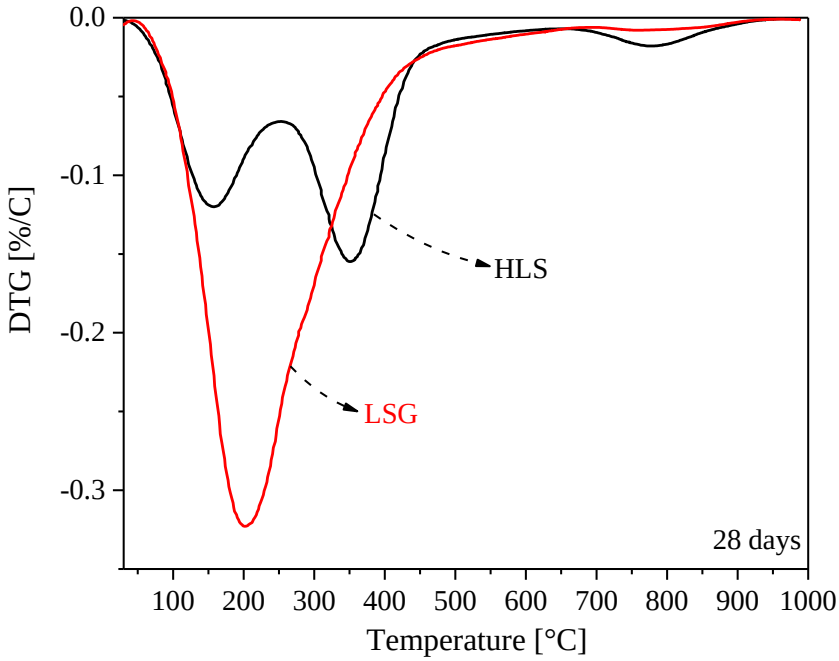

(b)

221 ***Figure 3. Thermal gravimetric analysis (TGA) of LSG and HLS mortar under heating***

222 ***scheme to 1000^{0}C at (a) 7 days and (b) 28 days***

223 SEM was used to observe the fractured surfaces of the samples at different ages (Figure 4).

224 LSG formed needle-like elongated crystals, which is typical of ettringite crystals' formation in

225 cement microstructures. Ettringite was found in the LSG with SEM observation and this was

226 in accordance to the expectation based on Equation 1. The crystal was a stable phase, thus there

227 were no conversion and microstructural changes. In contrast, the microstructure images of HLS

228 confirm the conversion process when comparing the observation on fracture surface at 7 and

229 28 days (see Figure 4b). At 7 days, the paste microstructure shows plate-like crystals, which

230 are consistent with C_2AH_8 [33,43,44]. However, at 28 days, the microstructure of fracture

231 surface for HLS contained finely shaped cubic crystals indicating C_3AH_6. This is in agreement

232 with a previous investigation on calcium aluminates cement [42]. Moreover, the microstructure
233 appears more porous compared to HLS microstructure at 7 days. The differences between HLS
234 and LSG, observed by SEM, is relevant with the XRD and TGA results shown in Figure 2 and
235 3 respectively.
236

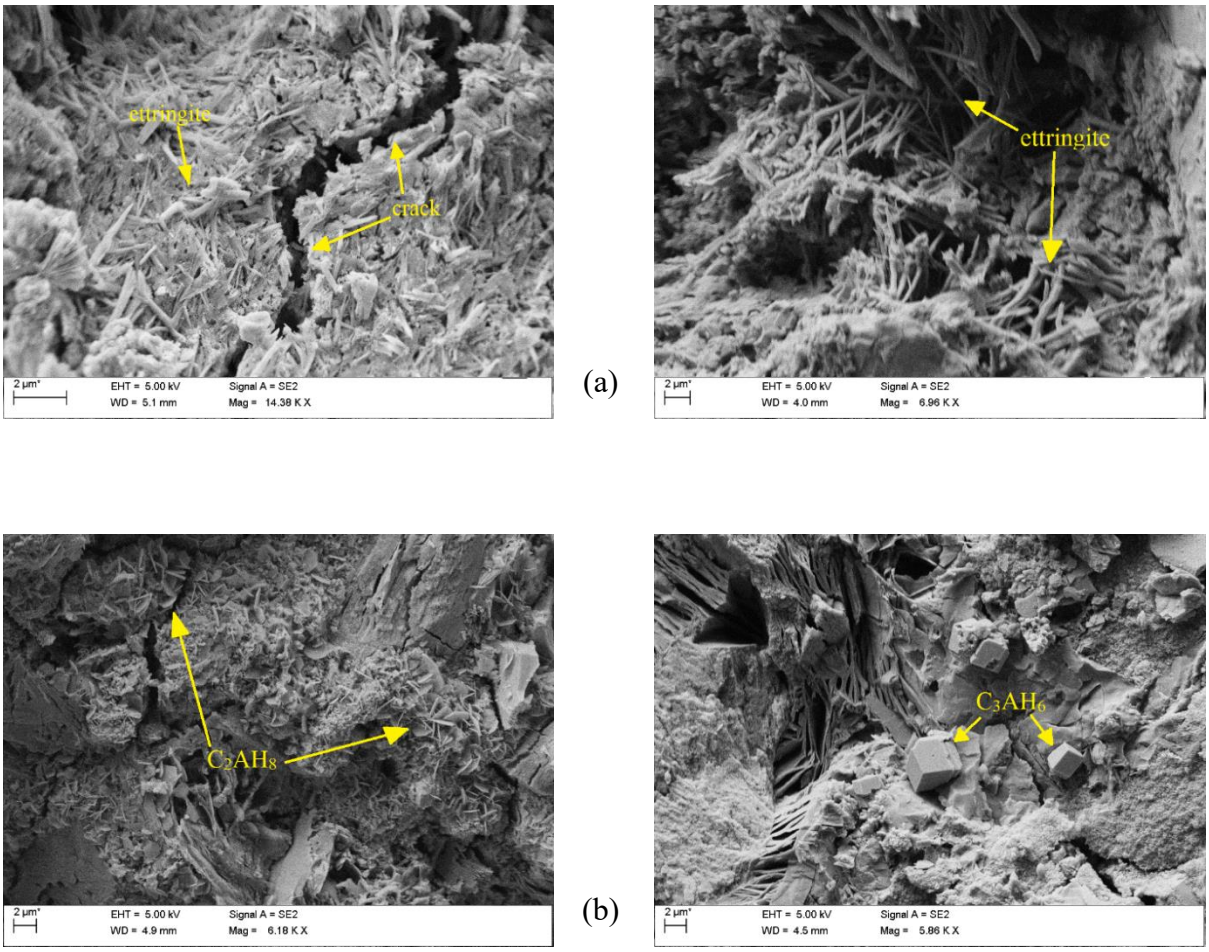

237 ***Figure 4. SEM images of LSG (a) and HLS (b) after 7 (left) and 28 (right) days of curing***

238 **3.2. Heat of hydration via isothermal calorimetry**

239 Isothermal calorimetry signal clearly distinguishes the heat evolved of LSG and HLS from
240 mixing of the slag to 50 hours of hydration. Figure 5 shows the heat evolution (J/h.g) and

cumulative heat released (J/g) curves for the first 50 hours of hydration of both HLS and LSG. For HLS, two distinct peaks can be observed as early dissolution peak and later acceleration peak. The initial peak for HLS is attributed to the wetting and dissolution of LS. The intensity of this initial heat is however lower than LSG's initial heat curve due to the combined heat evolved from gypsum with LS. After this initial peak, a short dormant period for HLS occurred and then a sharp increase to an acceleration peak with the highest peak occurring 5 hours after the start of the measurement. This high-intensity peak is attributed to the reaction of $C_{12}A_7$. Although $C_{12}A_7$ is a fast setting crystal, the hydration has, however, been retarded by the citric acid added, which contributed to the later acceleration peak starting after approximately 2 hours.

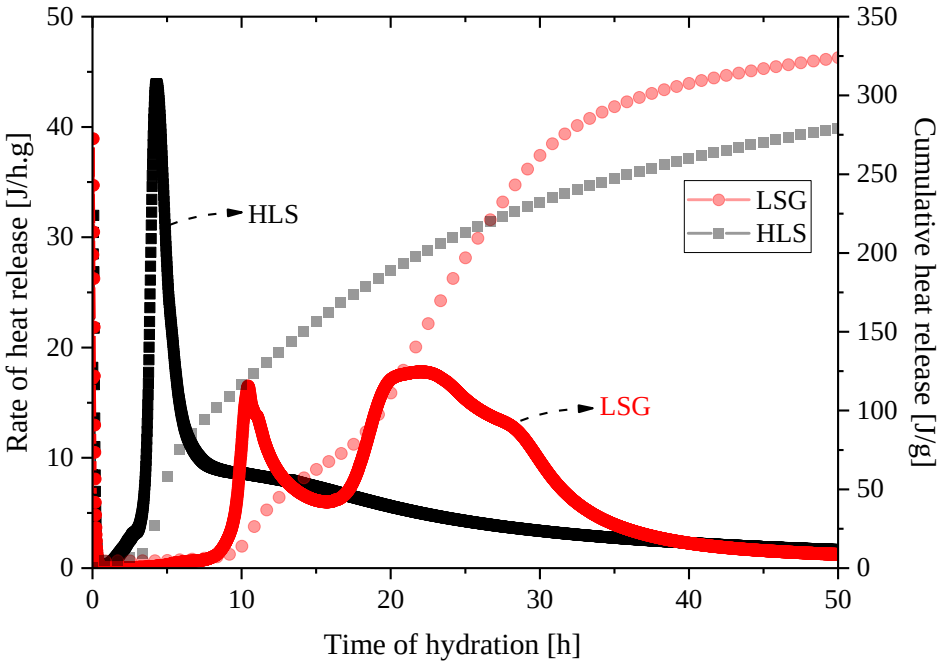

Figure 5. Isothermal calorimetry measurement for heat of hydration between LSG and HLS

LSG demonstrated three significant peaks of hydration and a shoulder on the third peak.

This heat evolution behavior indicates that the addition of gypsum had a significant effect on the hydration. The first peak was due to wetting and dissolution of gypsum-slag blends. After this initial peak, LSG experienced a longer dormant period lasting up to 8 hours because of the set retardation effects of both gypsum and citric acid in the paste. This period was then followed by a sharp acceleration that peaked at 10 hours after the start of the hydration, the heat evolved at this stage is attributed to the formation of ettringite in the gypsum-slag binder. The third peak is attributed to the second formation of ettringite. The shoulder with heat flow peak at 28 hrs of the deceleration peak is attributed to renewed dissolution of the anhydrous gypsum-slag cement, which possibly reacts with ettringite to form monosulfoaluminate. According to Quennoz [45], the third peak is suggested to be second formation of ettringite while the shoulder peak is caused by the formation of monosulfoaluminate consistent with the mineralogy in Figure 2a. In addition, the cumulative heat released curves (Figure 5) shows that LSG has the highest total heat evolved after 50 hours of hydration, which demonstrates the collective influence of gypsum addition to influencing the hydration of the LSG.

3.3. Mechanical and durability properties

3.3.1. Compressive and flexural strength

LSG achieved considerably high compressive strength at an early age, and the compressive strength at final curing age was 35 MPa. Figure 6a shows the compressive properties of the materials. At 7 days, the compressive strength of LSG gained 30 MPa, which was

approximately 85% of the compressive strength after 28 curing days. Similarly to other ettringite-based binders [17,18], LSG is a high-early-strength cementitious binder due to the rapid development of ettringite. In addition, it is worth mentioning that the compressive strength of LSG after 28 days of curing was relatively good (i.e., 35 MPa) and, hence, could be used in structural design codes (e.g., Euro code 2 [46]). In contrast, the compressive strength of HLS reduced after 28 days of curing due to the conversion of the metastable hydration products as reported in previous sections and in [8,37].

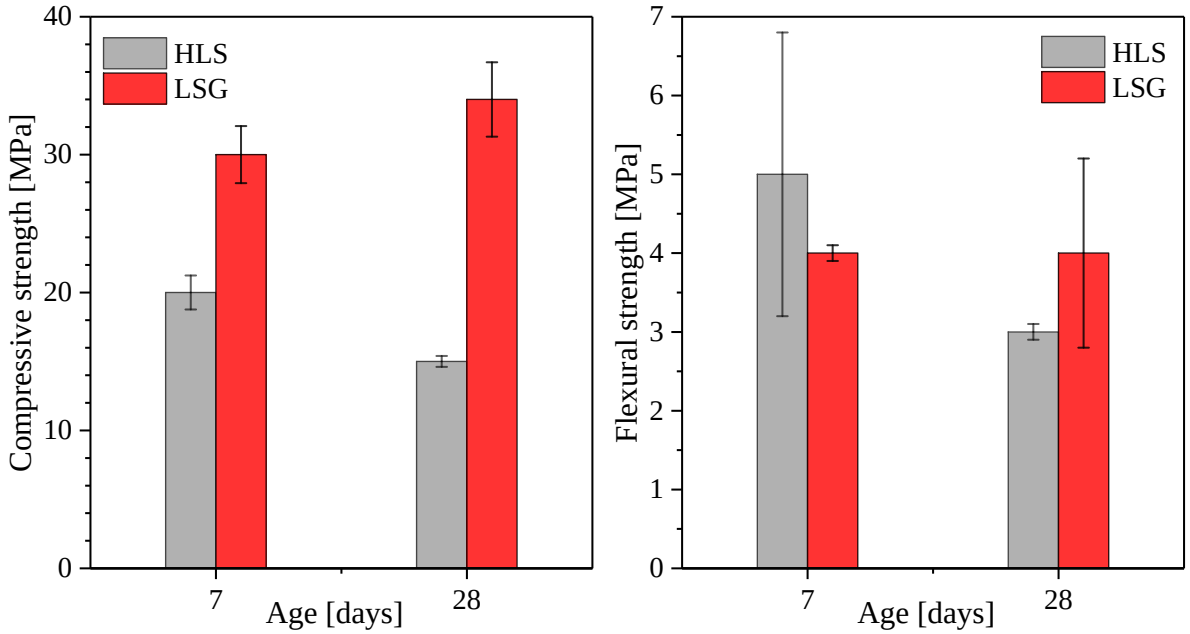

(a) (b)

Figure 6. Strength test: (a) compressive strength, (b) flexural strength at 7 and 28 days

The flexural strength of LSG was approximately 4 MPa, which is comparable with the ettringite-based binder developed in [47]; there was only minor change over time (Figure 6b). In contrast, the flexural strength of HLS dropped from early to final age by roughly 40%. As

284 suggested in [8], a method to reduce strength loss due to mineral conversion is needed.
285 Scrivener [48] suggested reducing the amount of water (water-to-binder ratio ≤ 0.4) to
286 minimize the conversion rate. Another possibility that requires more energy consumption is
287 through high temperature treatment and rapid cooling of the slag.

288 **3.3.2. Drying shrinkage**

289 The ettringite-based binder shrunk less than the hydrated LS. Figure 7 shows a comparison
290 in drying shrinkage between HLS and LSG in the observation of 90 days. The drying shrinkage
291 of LSG started at the early ages (3 days after casting) and stabilized from 7 days of curing
292 onward. Similar findings were reported in the literature [49,50]. In addition, the shrinkage of
293 LSG at 90 days was almost the same with that of 7 days, and the shrinkage level was relatively
294 low in comparison to HLS. This behavior is in agreement with the compressive strength of
295 LSG (see Figure 6a) where LSG formed ettringite rapidly within initial 24 hours, and
296 eventually there were no many changes in its structure later on. On the other hand, from day 3
297 to day 90, the shrinkage of HLS increased almost 5 times more than LSG; this might be due to
298 the mineral conversion of the metastable hydrates to a stable hydrate during the testing period.
299 This conversion phenomenon resulted a change in structural and volumetric properties of the
300 concrete. The metastable hydrate (C_2AH_8), which was formed initially at early age, has a
301 density (i.e., 1750 kg/m^3) different from that of C_3AH_6 (i.e., 2520 kg/m^3) [43]. This volumetric
302 difference led to a reduction in solid volume of the concrete as reported in [43]. This

phenomenon was accompanied by releasing water, which might have evaporated during the course of the test contributing to the shrinkage values recorded. In addition, no macro or micro cracks were observed on the concrete structure during the length change analysis. Consequently, the strength loss of HLS, as discussed in section 3.3.1, is in accordance to the high shrinkage rate. However, the shrinkage value of HLS is comparable to that of activated blast furnace slag cement reported in [49].

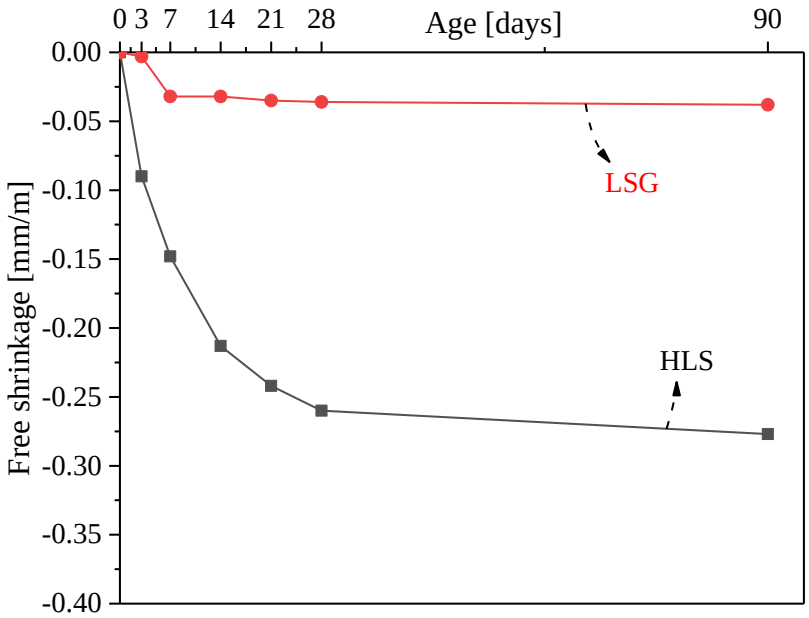

Figure 7. Drying shrinkage of LSG and HLS cured in air at RH 65% measured until 90 days

LSG shows similar shrinkage behavior with other ettringite-based binders. Ettringite is typically expansive; the crystal developed inside the capillary pores and hence produced an expansive force to reduce the shrinkage. Consequently, ettringite-based binders usually have very low shrinkage. Similar findings were reported in the literature. In [51], a composition of

316 aluminium-rich slag with gypsum, which formed ettringite in its structure, had the lowest
317 drying shrinkage due to the expansion tendency during early age. In [52,53], the
318 expansion/shrinkage of ettringite-based binder could be very low or almost negligible.
319 Therefore, in this investigation, the drying shrinkage of ettringite-based binder was in a good
320 agreement with other binders developed in [51,52]. However, further investigations on
321 micromechanics to understand the drying shrinkage of LSG is suggested.

322 **3.3.3. Freeze-thaw resistance**

323 After 300 freeze-thaw cycles, LSG showed much better material stability and less change
324 in mass than HLS. Figure 8 shows the material appearance and the mass loss of both HLS and
325 LSG after 300 cycles. LSG exhibits a great freeze-thaw resistance with just about 2% mass
326 change after 300 cycles. On the other hand, HLS indicates an inferior durability in which the
327 mass dropped and the shape of specimens changed significantly after 180 cycles. The
328 appearance and mass loss of samples are consistent with the residual strength of materials as
329 detailed in Figure 9.

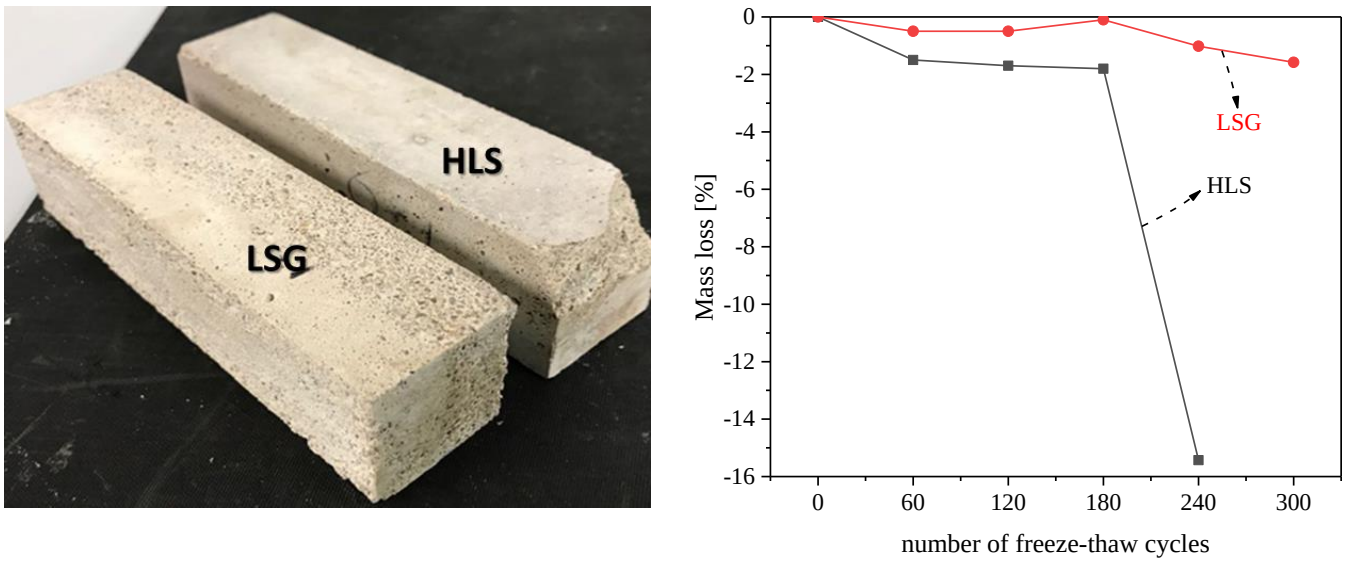

(a) (b)

330 ***Figure 8. Freeze-thaw test: (a) material appearance after 180 cycles and (b) mass change***

331 ***of LSG and HLS***

332 LSG shows a very good freeze-thaw resistance after 300 cycles (see Figure 9). After 300

333 cycles of freeze-thaw, LSG still attained a good residual compressive strength (i.e., 30 MPa) as

334 shown in Figure 9a; this compressive strength is satisfied with most of structure design codes

335 (e.g., [46]). Interestingly, the residual compressive strength of LSG after 120 cycles increased

336 by roughly 25% in comparison to the sample before aging. This is probably due to some further

337 reactions in the ettringite system in which water came into the material through micro cracks

338 and formed some new hydration products. After 120 freeze-thaw cycles, the compressive

339 strength of LSG decreased slightly, but still retained approximately 30 MPa compressive

340 strength. LSG had the residual strength after freezing and thawing as good as a fiber reinforced

341 composite reported in [54,55] or other calcium sulfoaluminate cement [56]. In contrast, HLS

shows a very poor resistance under freeze-thaw cycles; HLS samples failed after 240 cycles. The residual compressive strength dropped significantly (lower than 10 MPa) after 180 cycles and then failed before reaching the cycles of 240. Therefore, it can be clearly seen that LSG had much better durability than HLS under freeze-thaw conditions.

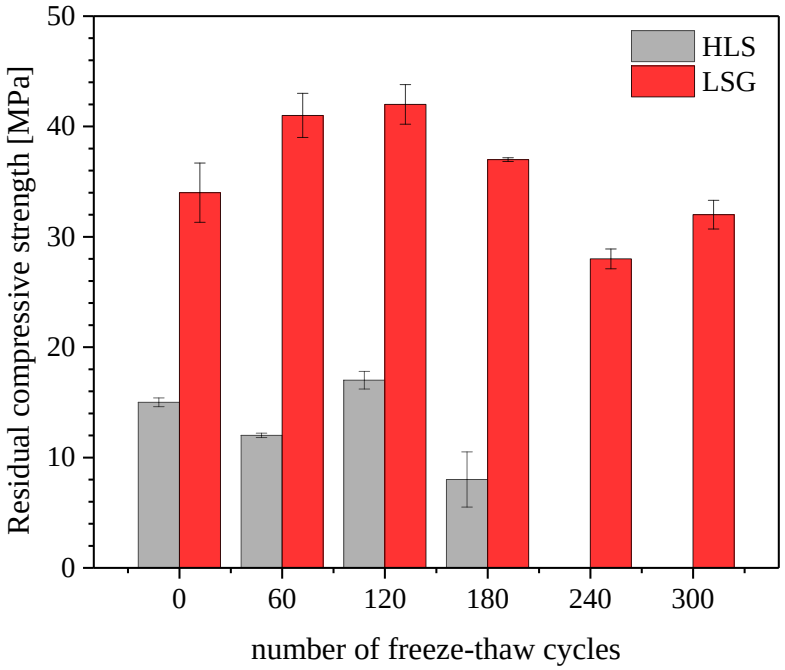

(a)

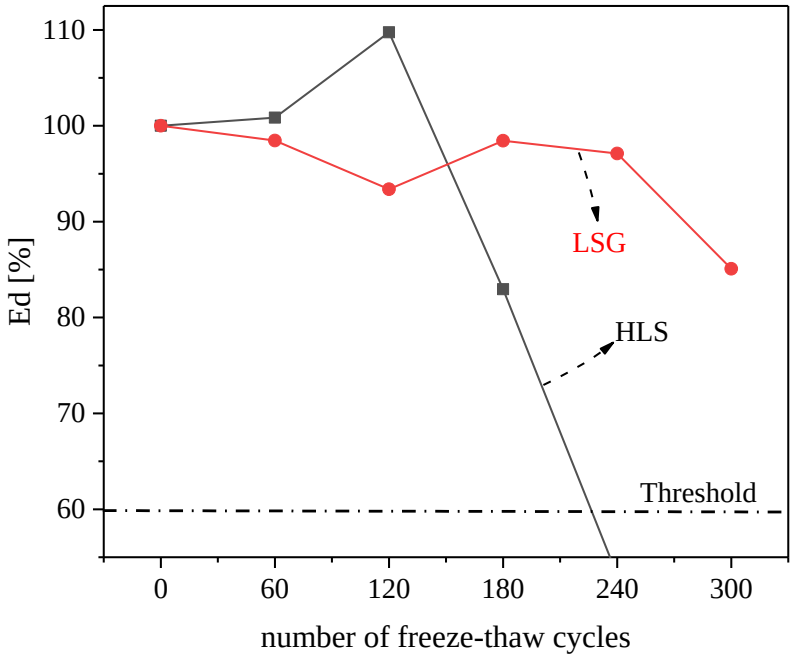

(b)

346 ***Figure 9. Freeze-thaw test: (a) residual compressive strength, (b) relative dynamic modulus***

347 ***elasticity (Ed) of LSG and HLS measured by UPV technique after freeze-thaw cycles***

348 The measurement of *Ed* by UPV confirms the good performance of LSG (see Figure 9b).

349 The threshold (60%) indicates the lower limit of measurement where the concrete is deemed

350 sub-standard and further analysis stopped [26]. The *Ed* of LSG generally decreased under

351 freeze-thaw process by 15% after F300. In addition, there was no significant difference among

352 samples from cycle 0 to cycle 240 in term of *Ed*; a good agreement was indicated in Figure 9a

353 for the residual compressive strength of LSG. As for HLS, the *Ed* dropped sharply after 180

354 cycles, which is also in the same trend with the residual strength of HLS. The measurement of

355 *Ed* has been used as an estimation and prediction of the mechanical properties and internal

356 damage of cement and concrete [57].

4. Conclusions

In this study, the properties of hydrated ladle slag and its modification with gypsum to form an ettringite-based binder were investigated. The experimental investigation indicated that LS can be employed effectively as a precursor for the ettringite-based binder (i.e., LSG) via hydrations between LS and gypsum. LS and gypsum can be utilized with a mass ratio of 70% and 30%, respectively, as an eco-cement. Ettringite is the main crystalline phase of the binder, providing relatively good compressive strength to LSG mortars (i.e., 35 MPa). The material was characterized by X-ray diffraction, thermogravimetric analysis, scanning electron microscope, and isothermal calorimetry to give better understanding of its mineralogical behavior.

The compressive strength of LSG developed rapidly and was roughly 30 and 35 MPa at 7 and 28 days of curing respectively. On the other hand, the flexural strength remained almost constant for the two curing ages. In addition, LSG showed much lower drying shrinkage than HLS and similar to other ettringite-based binders reported in the literature. Furthermore, LSG exhibited a superb freeze-thaw resistance in which the residual compressive strength after 300 cycles was almost the same with the material before testing (i.e., approximately 30 MPa). In contrast, during these same strength tests periods, HLS showed reduction in strength due to the conversion of hydration products from C_2AH_8 to C_3AH_6. Moreover, HLS exhibited much higher drying shrinkage, which might lead to micro cracks in the material, and poor freeze-

thaw resistance (failed in the test after 240 cycles).

The produced ettringite-based binder is a low-cost cementitious material that results from a synergistic reaction between byproduct-based raw materials (LS and gypsum); > 98% of the raw materials exist as byproducts with minor additives used for set retardation. The manufacturing process, hence, requires energy mainly for the grinding of the raw materials. Consequently, the manufacturing process is economically and environmentally promising.

Finally, this study provides the details and understanding of the byproduct-based ettringite binder from steel manufacturing byproducts. There is still work to be done, including whether there is conversion in LSG after a long period of time, durability of the material under aggressive environments (i.e., chloride and sulfate attack), and life-cycle assessment of the material.

Acknowledgement

This work is a part of MINSI project (A70189), which is supported by the European Regional Development Fund (ERDF), and various companies including Fortum Waste Solutions, Pohjolan Voima, Oulun Energia, SSAB Europe, and Stora Enso. Hoang Nguyen gratefully acknowledges the financial support from Tauno Tönning Foundation. Elijah Adesanya would like to acknowledge the Auramo-Saatio Foundation for the research grant towards his doctoral research.

References

[1] H.W. Kua, Integrated policies to promote sustainable use of steel slag for construction—A consequential life cycle embodied energy and greenhouse gas emission perspective, Energy Build. 101 (2015) 133–143. doi:10.1016/j.enbuild.2015.04.036.

[2] J. Guo, Y. Bao, M. Wang, Steel slag in China: Treatment, recycling, and management, Waste Manag. 78 (2018) 318–330. doi:10.1016/j.wasman.2018.04.045.

[3] Steel Statistical Yearbook 2017, Steel Stat. Yearb. 2010-2017. (2017). https://www.worldsteel.org/steel-by-topic/statistics/steel-statistical-yearbook-.html (accessed December 7, 2017).

[4] Y. Jiang, T.-C. Ling, C. Shi, S.-Y. Pan, Characteristics of steel slags and their use in cement and concrete—A review, Resour. Conserv. Recycl. 136 (2018) 187–197. doi:10.1016/j.resconrec.2018.04.023.

[5] Y.-N. Sheen, D.-H. Le, T.-H. Sun, Innovative usages of stainless steel slags in developing self-compacting concrete, Constr. Build. Mater. 101 (2015) 268–276. doi:10.1016/j.conbuildmat.2015.10.079.

[6] M. Tossavainen, F. Engstrom, Q. Yang, N. Menad, M. Lidstrom Larsson, B. Bjorkman, Characteristics of steel slag under different cooling conditions, Waste Management. 27 (2007) 1335–1344. doi:10.1016/j.wasman.2006.08.002.

[7] E. Adesanya, K. Ohenoja, P. Kinnunen, M. Illikainen, Alkali Activation of Ladle Slag from Steel-Making Process, J. Sustain. Metall. (2016) 1–11. doi:10.1007/s40831-016-0089-x.

[8] E. Adesanya, K. Ohenoja, P. Kinnunen, M. Illikainen, Properties and durability of alkali-activated ladle slag, Mater. Struct. 50 (2017) 255. doi:10.1617/s11527-017-1125-4.

[9] R. Ji, Y. He, Z. Zhang, L. Liu, X. Wang, Preparation and modeling of energy-saving building materials by using industrial solid waste, Energy Build. 97 (2015) 6–12. doi:10.1016/j.enbuild.2015.02.015.

[10] A. Natali Murri, W.D.A. Rickard, M.C. Bignozzi, A. van Riessen, High temperature behaviour of ambient cured alkali-activated materials based on ladle slag, Cem. Concr. Res. 43 (2013) 51–61. doi:10.1016/j.cemconres.2012.09.011.

[11] P. Duxson, J.L. Provis, G.C. Lukey, J.S.J. van Deventer, The role of inorganic polymer technology in the development of ‘green concrete,’ Cem. Concr. Res. 37 (2007) 1590–1597. doi:10.1016/j.cemconres.2007.08.018.

[12] J.S.J. van Deventer, J.L. Provis, P. Duxson, D.G. Brice, Chemical Research and Climate Change as Drivers in the Commercial Adoption of Alkali Activated Materials, Waste Biomass Valorization. 1 (2010) 145–155. doi:10.1007/s12649-010-9015-9.

[13] B.C. McLellan, R.P. Williams, J. Lay, A. van Riessen, G.D. Corder, Costs and carbon emissions for geopolymer pastes in comparison to ordinary portland cement, J. Clean.

Prod. 19 (2011) 1080–1090. doi:10.1016/j.jclepro.2011.02.010.
[14] A. Peys, L. Arnout, B. Blanpain, H. Rahier, K. Van Acker, Y. Pontikes, Mix-design Parameters and Real-life Considerations in the Pursuit of Lower Environmental Impact Inorganic Polymers, Waste Biomass Valorization. 9 (2018) 879–889. doi:10.1007/s12649-017-9877-1.
[15] L.K. Turner, F.G. Collins, Carbon dioxide equivalent (CO2-e) emissions: A comparison between geopolymer and OPC cement concrete, Constr. Build. Mater. 43 (2013) 125–130. doi:10.1016/j.conbuildmat.2013.01.023.
[16] A. Passuello, E.D. Rodríguez, E. Hirt, M. Longhi, S.A. Bernal, J.L. Provis, A.P. Kirchheim, Evaluation of the potential improvement in the environmental footprint of geopolymers using waste-derived activators, J. Clean. Prod. 166 (2017) 680–689. doi:10.1016/j.jclepro.2017.08.007.
[17] A. Rungchet, P. Chindaprasirt, S. Wansom, K. Pimraksa, Hydrothermal synthesis of calcium sulfoaluminate–belite cement from industrial waste materials, J. Clean. Prod. 115 (2016) 273–283. doi:10.1016/j.jclepro.2015.12.068.
[18] R.X. Magallanes-Rivera, J.I. Escalante-García, Anhydrite/hemihydrate-blast furnace slag cementitious composites: Strength development and reactivity, Constr. Build. Mater. 65 (2014) 20–28. doi:10.1016/j.conbuildmat.2014.04.056.
[19] J.-M. Kim, S.-M. Choi, D. Han, Improving the mechanical properties of rapid air cooled ladle furnace slag powder by gypsum, Constr. Build. Mater. 127 (2016) 93–101. doi:10.1016/j.conbuildmat.2016.09.102.
[20] European Standard, EN 450-1, Fly ash for concrete. Definition, specifications and conformity criteria, European Standard, 2012.
[21] ISO 13320:2009 - Particle size analysis -- Laser diffraction methods, International Organization for Standardization, 2009.
[22] L. Gobbo, L. Sant'Agostino, L. Garcez, C3A polymorphs related to industrial clinker alkalies content, Cem. Concr. Res. 34 (2004) 657–664. doi:10.1016/j.cemconres.2003.10.020.
[23] ASTM International, ASTM C191-13, Standard Test Methods for Time of Setting of Hydraulic Cement by Vicat Needle, ASTM International, West Conshohocken, PA, 2013. www.astm.org.
[24] SFS (Finnish Standards Association), "Methods of testing cement. Part 1: Determination of strength" SFS-EN 196-1:2016:en, 2016.
[25] ASTM International, ASTM C596 - 09(2017), Standard Test Method for Drying Shrinkage of Mortar Containing Hydraulic Cement, ASTM International, West Conshohocken, PA, 2017. www.astm.org.
[26] ASTM C666 / C666M - 15 Standard Test Method for Resistance of Concrete to Rapid Freezing and Thawing, (n.d.). https://www.astm.org/Standards/C666.htm (accessed

January 3, 2017).
[27] S.A. Omer, R. Demirboga, W.H. Khushefati, Relationship between compressive strength and UPV of GGBFS based geopolymer mortars exposed to elevated temperatures, Constr. Build. Mater. 94 (2015) 189–195. doi:10.1016/j.conbuildmat.2015.07.006.
[28] R. Ghosh, S.P. Sagar, A. Kumar, S.K. Gupta, S. Kumar, Estimation of geopolymer concrete strength from ultrasonic pulse velocity (UPV) using high power pulser, J. Build. Eng. 16 (2018) 39–44. doi:10.1016/j.jobe.2017.12.009.
[29] R. Zaharieva, F. Buyle-Bodin, E. Wirquin, Frost resistance of recycled aggregate concrete, Cem. Concr. Res. 34 (2004) 1927–1932. doi:10.1016/j.cemconres.2004.02.025.
[30] I. Vegas, J. Urreta, M. Frías, R. García, Freeze–thaw resistance of blended cements containing calcined paper sludge, Constr. Build. Mater. 23 (2009) 2862–2868. doi:10.1016/j.conbuildmat.2009.02.034.
[31] I.F. Sáez del Bosque, S. Martínez-Ramírez, M.T. Blanco-Varela, Calorimetric study of white portland cement hydration. Effect of nanosilica and temperature, (2015). https://digital.csic.es/handle/10261/136074 (accessed November 9, 2018).
[32] J. Chang, Y. Zhang, X. Shang, J. Zhao, X. Yu, Effects of amorphous AH3 phase on mechanical properties and hydration process of C4A3S¯-CS¯H2-CH-H2O system, Constr. Build. Mater. 133 (2017) 314–322. doi:10.1016/j.conbuildmat.2016.11.111.
[33] C. Bradbury, P.M. Callaway, D.D. Double, The conversion of high alumina cement/concrete, Mater. Sci. Eng. 23 (1976) 43–53. doi:10.1016/0025-5416(76)90085-9.
[34] H.G. Midgley, A. Midgley, The conversion of high alumina cement, Mag. Concr. Res. 27 (1975) 59–77. doi:10.1680/macr.1975.27.91.59.
[35] K.L. Scrivener, J.-L. Cabiron, R. Letourneux, High-performance concretes from calcium aluminate cements, Cem. Concr. Res. 29 (1999) 1215–1223. doi:10.1016/S0008-8846(99)00103-9.
[36] M.A. Chavda, S.A. Bernal, D.C. Apperley, H. Kinoshita, J.L. Provis, Identification of the hydrate gel phases present in phosphate-modified calcium aluminate binders, Cem. Concr. Res. 70 (2015) 21–28. doi:10.1016/j.cemconres.2015.01.007.
[37] E. Adesanya, H. Sreenivasan, A.M. Kantola, V.-V. Telkki, K. Ohenoja, P. Kinnunen, M. Illikainen, Ladle slag cement – Characterization of hydration and conversion, Constr. Build. Mater. 193 (2018) 128–134. doi:10.1016/j.conbuildmat.2018.10.179.
[38] H. El-Didamony, Application of differential thermogravimetry to the hydration of expansive cement pastes, Thermochim. Acta. 35 (1980) 201–209. doi:10.1016/0040-6031(80)87194-2.
[39] W. Sha, G.B. Pereira, Differential scanning calorimetry study of hydrated ground granulated blast-furnace slag, Cem. Concr. Res. 31 (2001) 327–329. doi:10.1016/S0008-8846(00)00472-5.
[40] N.C. Collier, Transition and decomposition temperatures of cement phases – A collection

of thermal analysis data, Ceram. - Silik. (2016) 1–10. doi:10.13168/cs.2016.0050.
[41] K. De Weerdt, K.O. Kjellsen, E. Sellevold, H. Justnes, Synergy between fly ash and limestone powder in ternary cements, Cem. Concr. Compos. 33 (2011) 30–38. doi:10.1016/j.cemconcomp.2010.09.006.
[42] B. Pacewska, M. Nowacka, Studies of conversion progress of calcium aluminate cement hydrates by thermal analysis method, J. Therm. Anal. Calorim. 117 (2014) 653–660. doi:10.1007/s10973-014-3804-5.
[43] K.L. Scrivener, A. Capmas, 13 - Calcium Aluminate Cements A2 - Hewlett, Peter C., in: Leas Chem. Cem. Concr. Fourth Ed., Butterworth-Heinemann, Oxford, 1998: pp. 713–782. doi:10.1016/B978-075066256-7/50025-4.
[44] P. Barnes, J. Bensted, Structure and Performance of Cements, Second Edition, Chapter 4, CRC Press, 2002.
[45] A. Quennoz, Hydration of C3A with Calcium Sulfate Alone and in the Presence of Calcium Silicate, (2011). doi:10.5075/epfl-thesis-5035.
[46] European Union, EN 1992-1-1:2004 - Design of concrete structures. General rules and rules for buildings, The European Union, Avenue Marnix 17, B-1000, Brussels, Belgium, 2004.
[47] X. Wang, Z. Shui, R. Yu, M. Bao, G. Wang, Effect of coral filler on the hydration and properties of calcium sulfoaluminate cement based materials, Constr. Build. Mater. 150 (2017) 459–466. doi:10.1016/j.conbuildmat.2017.05.194.
[48] K. Scrivener, Calcium aluminate cements, in: Adv. Concr. Technol. 1 Const. Mater., Butterworth-Heinemann, Oxford, 2003: p. P2/2-2/19.
[49] B.S. Cho, H.H. Lee, Y.C. Choi, Effects of aluminate rich slag on compressive strength, drying shrinkage and microstructure of blast furnace slag cement, Constr. Build. Mater. 140 (2017) 293–300. doi:10.1016/j.conbuildmat.2017.02.111.
[50] S. Aydın, B. Baradan, Effect of activator type and content on properties of alkali-activated slag mortars, Compos. Part B Eng. 57 (2014) 166–172. doi:10.1016/j.compositesb.2013.10.001.
[51] M. García-Maté, A.G. De la Torre, L. León-Reina, E.R. Losilla, M.A.G. Aranda, I. Santacruz, Effect of calcium sulfate source on the hydration of calcium sulfoaluminate eco-cement, Cem. Concr. Compos. 55 (2015) 53–61. doi:10.1016/j.cemconcomp.2014.08.003.
[52] I. Janotka, L. Krajči, A. Ray, S.. Mojumdar, The hydration phase and pore structure formation in the blends of sulfoaluminate-belite cement with Portland cement, Cem. Concr. Res. 33 (2003) 489–497. doi:10.1016/S0008-8846(02)00994-8.
[53] A. Telesca, M. Marroccoli, M.L. Pace, M. Tomasulo, G.L. Valenti, P.J.M. Monteiro, A hydration study of various calcium sulfoaluminate cements, Cem. Concr. Compos. 53 (2014) 224–232. doi:10.1016/j.cemconcomp.2014.07.002.

[54] H.-D. Yun, K. Rokugo, Freeze-thaw influence on the flexural properties of ductile fiber-reinforced cementitious composites (DFRCCs) for durable infrastructures, Cold Reg. Sci. Technol. 78 (2012) 82–88. doi:10.1016/j.coldregions.2012.02.002.

[55] J. Nam, G. Kim, B. Lee, R. Hasegawa, Y. Hama, Frost resistance of polyvinyl alcohol fiber and polypropylene fiber reinforced cementitious composites under freeze thaw cycling, Compos. Part B Eng. 90 (2016) 241–250. doi:10.1016/j.compositesb.2015.12.009.

[56] L. Li, R. Wang, Q. Lu, Influence of polymer latex on the setting time, mechanical properties and durability of calcium sulfoaluminate cement mortar, Constr. Build. Mater. 169 (2018) 911–922. doi:10.1016/j.conbuildmat.2018.03.005.

[57] G. Trtnik, F. Kavcic, G. Turk, Prediction of concrete strength using ultrasonic pulse velocity and artificial neural networks, Ultrasonics. 49 (2009) 53–60. doi:10.1016/j.ultras.2008.05.001.